Available online at www.sciencedirect.com
SCIENCE DIRECT®
ELSEVIER
Journal of the European Ceramic Society 25 (2005) 1733–1742
ECERS
www.elsevier.com/locate/jeurceramsoc

Electron microscopy study on the high-temperature oxidation of Si_3N_4–TiN ceramics: in situ and ex situ investigations

Armin Feldhoff*,[1], Marie-France Trichet, Leo Mazerolles, Monika Backhaus-Ricoult[2]

Centre d'Etudes de Chimie Métallurgique CNRS, UPR2801, 15, rue George Urbain, F-94407 Vitry sur Seine, France

Available online 15 January 2005

Abstract

The high-temperature oxidation of Si_3N_4–TiN particulate composites with different amounts of the glass forming sinter additives Al_2O_3 and Y_2O_3 has been studied in order to reveal the oxidation mechanism with its different reaction steps and kinetics and especially identify the role of the glass phase in the course of oxidation. The initial stages of oxidation have been observed in situ in an environmental scanning electron microscope while exposing the materials to dry or humid oxidation environment at temperatures between 600 and 1100 °C. For the characterization of the later oxidation stages, materials were oxidized ex situ for longer times. The oxidation scales were characterized by X-ray diffraction, field emission scanning electron microscopy and transmission electron microscopy.

Oxidation of the composites starts at 650 °C, when TiN surface particles begin to oxidize and form on their exposed surface islands of nanocrystalline TiO_2. At around 950 °C, the glass transition temperature of the intergranular glass phase, these nanocrystals start to grow laterally on the surface. At the same time, oxidation progresses into the depth of the material, forming thereby several distinguished oxidation subscales. The intergranular glass plays a crucial role for the oxidation in the temperature range between 950 and 1100 °C. Depending on the glass quantity in presence, different reaction mechanisms dominate; the oxidation kinetics are strongly controlled by the transport within the intergranular glass.

Keywords: Composites; Electron microscopy; Corrosion; Si_3N_4; TiN

1. Introduction

Compared to monolithic silicon nitride ceramics, silicon nitride–titanium nitride composites exhibit an improved fracture toughness and are machinable by electric discharge, thus providing the possibility to realize ceramic parts of complex shape.[1–4] These properties make the composite a suitable high-temperature structural material, however, its corrosion resistance at temperatures above 1000 °C is reported to be poor compared to that of pure silicon nitride ceramics. For silicon nitride ceramics, the oxidation resistance depends strongly on quality and quantity of the sinter additives and can be tremendously improved by carefully designing the microstructure.[5–7] To predict and improve the performance of the much more complicated Si_3N_4–TiN materials in high-temperature services, a fundamental knowledge of the oxidation mechanism is needed. In the past, several studies showed that the oxidation mechanism is complex, and multilayered scales form.[8–12] The initial oxidation stages of Si_3N_4–TiN ceramics have not yet been studied. Thus, it remains unknown, where and how oxidation starts and whether the first stages of oxidation vary with temperature, environment, quality and quantity of sinter additives. The aim of the present work is to study these very initial stages of oxidation by in situ observation in an environmental scanning electron microscope and thus contribute to the understanding of the interplay of nucleation, growth and transport in the formation of the early oxidation products.

* Corresponding author. Tel.: +49 511 762 2940.
E-mail address: armin.feldhoff@pci.uni-hannover.de (A. Feldhoff).
[1] Present address: Institut für Physikalische Chemie und Elektrochemie, Universität Hannover, Callinstraße 3-3A, D-30167 Hannover, Germany.
[2] Present address: Corning Incorporated, Crystalline Materials Group, S&T, Sullivan Park SP AR 02, Corning, NY 14831, USA.

0955-2219/$ – see front matter © 2004 Elsevier Ltd. All rights reserved.
doi:10.1016/j.jeurceramsoc.2004.12.003

2. Experimental

Two Si_3N_4-based composites with 35 vol.% of TiN and different amounts of sinter additives were studied: Composite A is an uniaxially hot-pressed ceramic with a high level of sintering additives (2.5 wt.% Al_2O_3, 5 wt.% Y_2O_3, 1800 °C, 30 MPa), and composite B an hot-isostatically pressed composite with a lower level of additives (0.25 wt.% Al_2O_3, 0.5 wt.% Y_2O_3, 1725 °C, 150 MPa). Oxidation treatments were realized in an environmental scanning electron microscope (ESEM-3, Electroscan, Wilmington, MA, USA) equipped with a hot-stage. The latter was specified for operation between room temperature and 1500 °C. Specimens with the dimension 1 mm × 2 mm × 2 mm with a mirror-finished surface were used for the in situ oxidation in the ESEM. Different atmospheres were established in the ESEM during oxidation for up to 2 h: a humid environment, in which air was saturated with water at 18 °C ($p(H_2O)$ = 2 kPa) and a dry environment of pure oxygen at a total pressure of 265 Pa, respectively. In addition, both composites were oxidized for longer times (between 4 and 100 h) in a high-temperature furnace with an alumina tubing under the flow of dried or humified air ($p(H_2O)$ = 2 kPa). The surface of oxidized samples was analyzed by X-ray diffraction (XRD) using Co Kα radiation on a Philips PW1830. Surfaces and cross sections were sputter-coated with an Au–Pd alloy and examined in a field-emission scanning electron microscope (FE-SEM), model Leo Gemini 1530 equipped with an energy-dispersive X-ray spectrometer (EDXS). Cross sections for SEM and transmission electron microscopy (TEM) were polished on diamond encrusted sheets with grain sizes between 30 and 0.1 μm. Final thinning of TEM specimen was done by ion milling under an argon beam. TEM investigations in bright- and dark-field mode were conducted at 120 kV in a JEOL 1200 EX and at 200 kV in a JEOL 2000 EX. High-resolution microscopy (HREM) was conducted at 200 kV in an Akashi Topcon that provides a point-resolution of 0.18 nm.

3. Results and discussion

3.1. As-sintered ceramics

The composite materials A and B both have a Si_3N_4 matrix, but contain different amounts of Al_2O_3 and Y_2O_3 as sinter additives. The second phase in both composites consists of 35 vol.% of micrometer sized TiN particles: Fig. 1a shows a backscattered electron (BSE) micrograph of a polished section of composite A. Due to the higher atomic number of titanium, the TiN particles appear in grey contrast compared to the Si_3N_4 matrix in dark contrast. Already in Fig. 1a, some bright contrast features from the relatively thick grain bound-

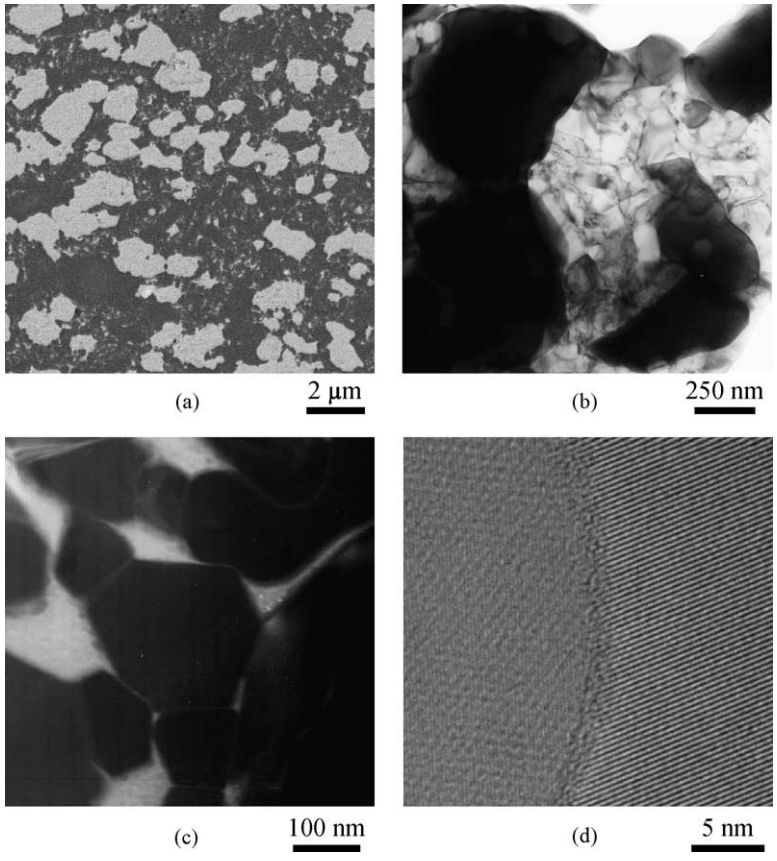

Fig. 1. (a) BSE image of composite A, (b) TEM bright-field of composite A, (c) TEM dark-field of composite A, and (d) HREM of composite B.

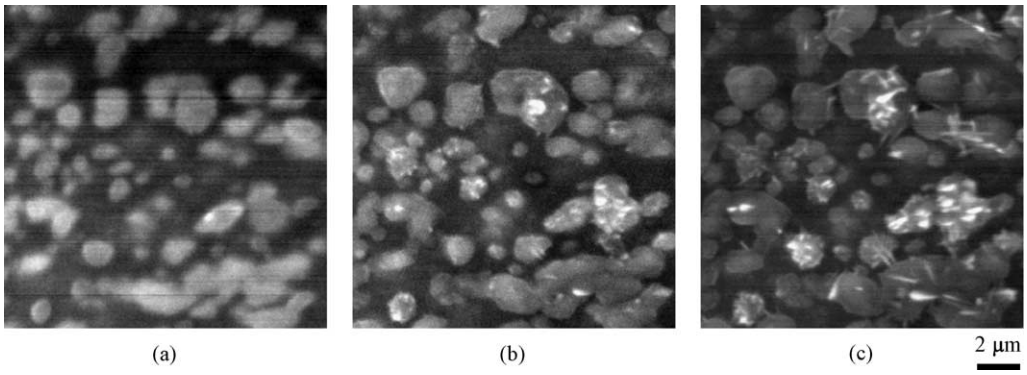

Fig. 2. Localized oxidation of TiN particles (light grey) at the surface of composite A during a temperature ramp of approximately 1.5 °C/min under dry air. (a) 600 °C, (b) 650 °C, (c) 700 °C.

ary film in the Si_3N_4 matrix can be distinguished which contains yttrium ($Z = 39$) and aluminium ($Z = 13$) from the sintering aids. The distribution of the intergranular glass shows that the grain size of silicon nitride is much smaller than that of titanium nitride. This is even more evident from the TEM bright-field (BF) image in Fig. 1b, in which TiN grains appear dark and the smaller silicon nitride grains appear bright. The silicon nitride grain size is in the order of 100–200 nm in both composites. The TEM dark-field (DF) image of composite A in Fig. 1c shows several well faceted silicon nitride grains (dark contrast) that are surrounded by the glassy grain boundary phase (homogeneous bright contrast). The glass film in composite A measures more than 10 nm in thickness along the grain boundaries and up to 100 nm in triple points. In composite B, the film width is smaller by a factor of 10. This difference is related to the different levels of sinter additives. The high-resolution TEM micrograph in Fig. 1d shows a typical grain boundary in the silicon nitride matrix of composite B. In the grain on the right side, $(1\,1\,\underline{2}\,0)$ lattice fringes of β-Si_3N_4 are visible with an interplanar distance of 0.38 nm. The grain boundary film width amounts to about 1.5 nm.

In summary, composites A and B have similar microstructures with respect to size and distribution of titanium nitride and silicon nitride. They are different in the thickness of their intergranular glass films which is a consequence of the different contents of sinter additives Al_2O_3 and Y_2O_3.

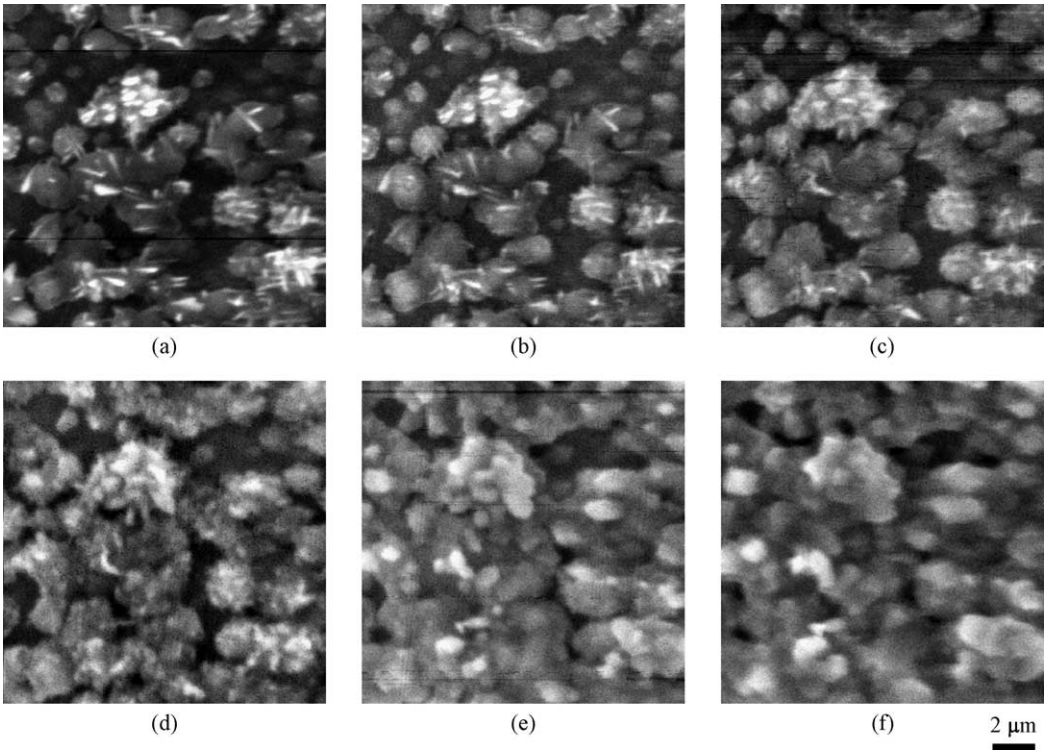

Fig. 3. Evolution of surface scale on composite A during a temperature ramp of approximately 1.5 °C/min under dry air. (a) 750 °C, (b) 800 °C, (c) 900 °C, (d) 950 °C, (e) 1000 °C for 5 min, (f) 1000 °C for 15 min.

3.2. In situ oxidation

Surfaces of composite A at various early stages of oxidation are presented in Figs. 2 and 3. The composite was oxidized in situ in the ESEM, at the starting temperature of 500 °C and a temperature ramp of approximately 1.5 °C/min. Fig. 2a shows the polished surface of composite A at 600 °C in dry air. The TiN particles appear in light grey and the silicon nitride matrix in dark contrast. First surface modifications were noticed at 650 °C (Fig. 2b) with the appearance of small nanocrystals (bright spots) on the exposed outer surface of the micrometer-sized TiN grains. At 700 °C (Fig. 2c), these nanocrystals grew to thin platelets with their long axis reaching micrometer dimensions. The surface of the silicon nitride matrix (dark contrast) remained unchanged. At 750, 800, and 900 °C (Fig. 3a–c) the nanocrystals on the TiN particles grew further in size, and some of them lost their platelike shape. The silicon nitride matrix surface areas remained still unchanged. At a threshold temperature of about 950 °C (Fig. 3d), the surface scale started to grow laterally over the silicon nitride matrix regions. At 1000 °C (Fig. 3e and f), lateral growth continued and grains in the scale coarsened visibly.

X-ray diffractograms (XRD) of oxidized composites showed a mixture of rutile (TiO_2), TiN and β-Si_3N_4 in the surface scales. The last two phases belong to the underlying non-oxidized composite. Thus, it is concluded that the nanocrystals on the outer surface of TiN particles are rutile. This was confirmed by EDXS and selected area electron diffraction in the TEM. Shape changes and coarsening of the nanocrystalline rutile during oxidation at temperatures above 950 °C suggest that a dissolution and reprecipitation process takes place that involves a glassy medium.

Fig. 4 illustrates the evolution of the surface scale of composite A with time at 1000 °C under humid air at a lower magnification. The lateral coalescence of the TiO_2 surface scale can be seen clearly in Fig. 4a–c. In the regions that are encircled in Fig. 4c some inhomogeneities (bright contrast) appear in the grain boundary phase of the silicon nitride matrix, which were identified as Ti-rich precipitates. For clarity, the encircled regions of Fig. 4c are shown in Fig. 4d–f at a higher magnification, and some of the precipitates are marked by arrows. The appearance of such precipitates in the vitreous grain boundary film indicates that, at 1000 °C, the intergranular glass is involved in the oxidation process. It should also be recalled that coalescence of rutile grains in the surface scale starts at almost the same temperature, 950 °C. The latter temperature matches well with typical glass transition temperatures reported for Y-Si-Al-O-N glasses.[13–15]

The coalescence of the crystals in the surface scale of composite A at 1100 °C under humid air is shown in Fig. 5. With time the TiO_2 layer gradually covered all silicon nitride matrix (dark contrast in Fig. 5a). In an early oxidation stage (Fig. 5a), rutile crystals were only several hundred nanometers in size. With time, they grew in size and developed pronounced crystal facets. After approximately 36 min (Fig. 5e), the surface was completely covered by a dense scale.The almost equiaxial rutile grains continued to coarsen and formed more pronounced facets. After 1 h at 1100 °C, TiO_2 grains in the dense scale reached sizes of several micrometers.

Composite B with the low level of additives behaved in most aspects similar to composite A. After a few minutes at 1000 °C in humid air (Fig. 6a) the silicon nitride surface still remained partially uncovered (dark contrast). As in composite A, the TiO_2 scale was composed of a mixture of equiaxial grains of several hundred nanometers in size and plate-like

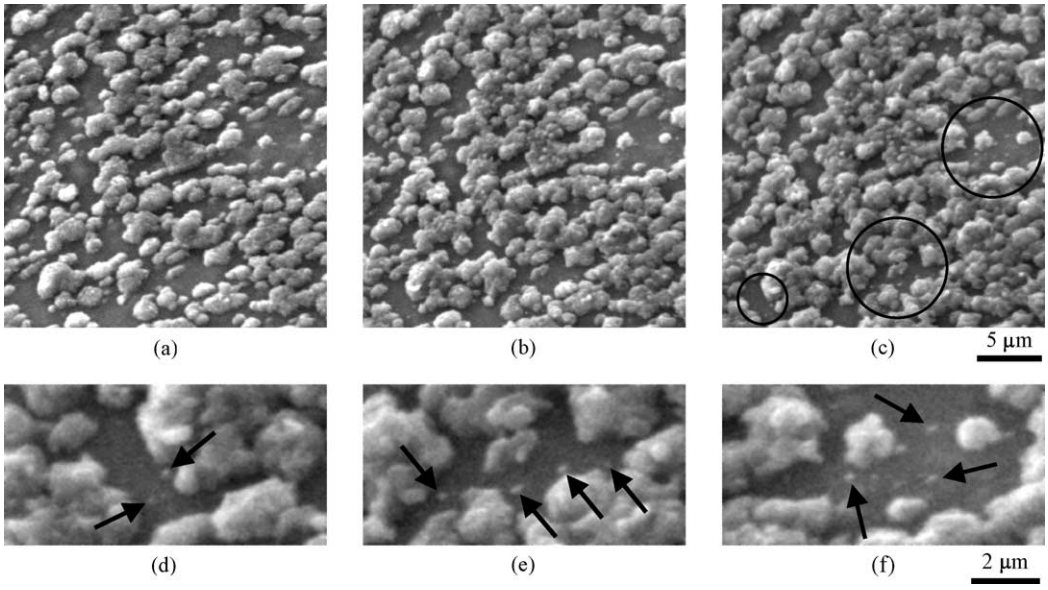

Fig. 4. Time sequence showing the surface scale on composite A at 1000 °C under humid air. (a) 6 min, (b) 19 min, (c) 34 min, (d–f) sections of encircled areas of panel c at a higher magnification.

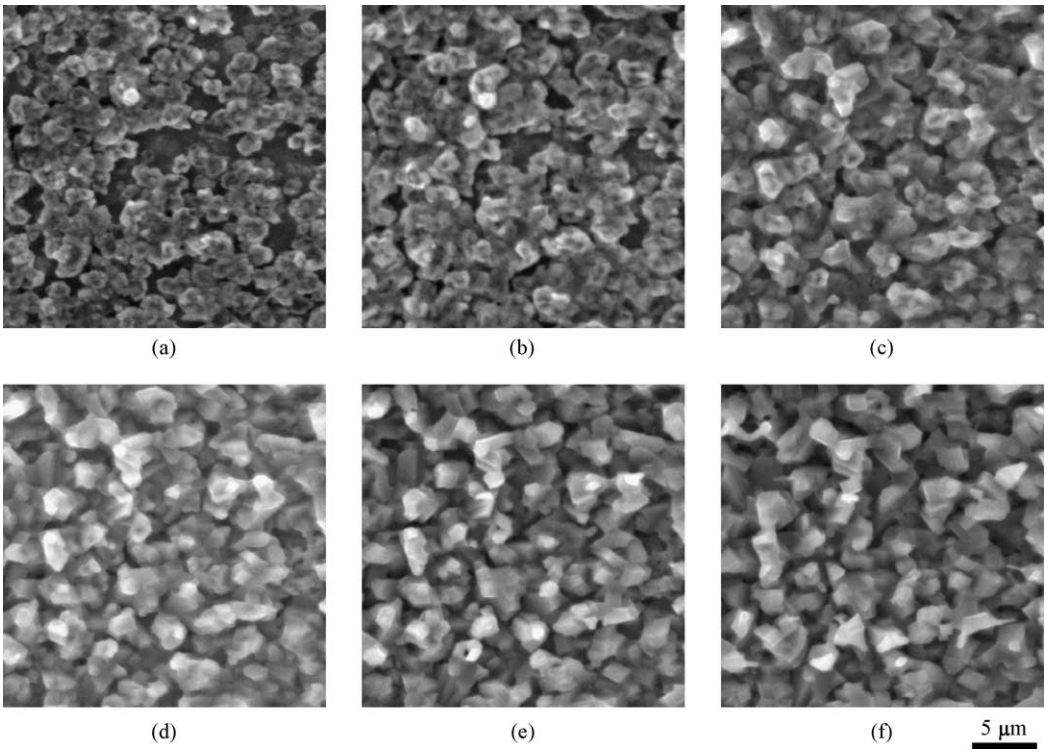

Fig. 5. Coalescence of surface scale on composite A at 1100 °C under humid air. (a) 3 min, (b) 7 min, (c) 16 min, (d) 22 min, (e) 36 min, (f) 56 min.

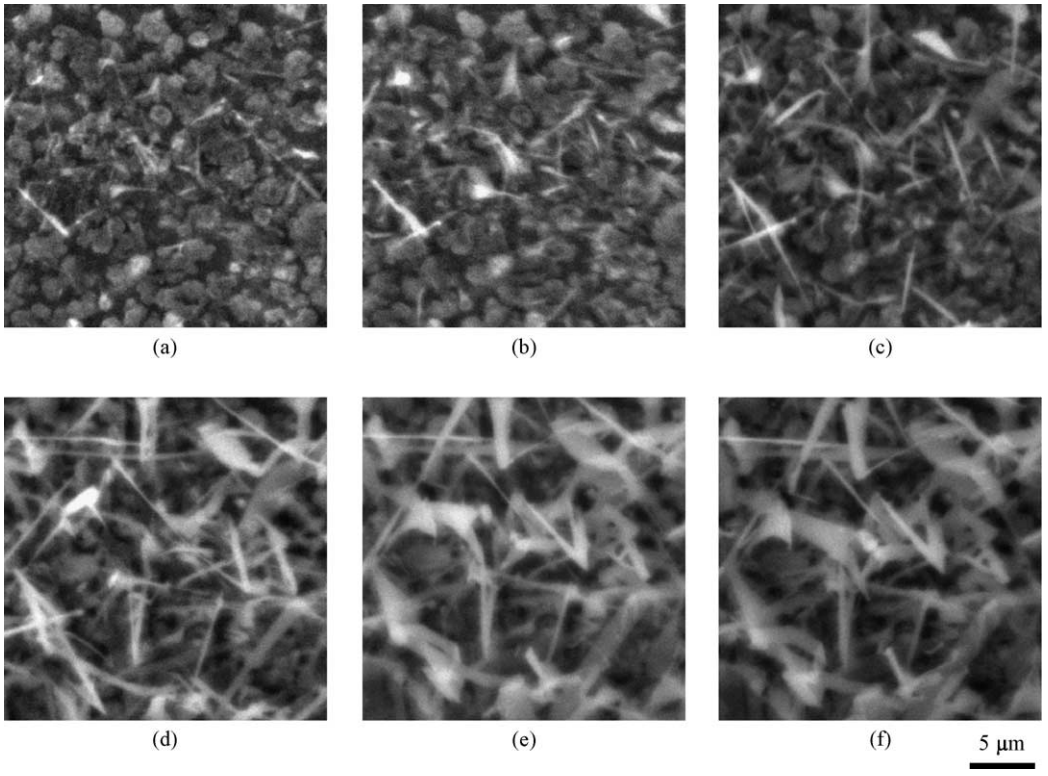

Fig. 6. Evolution of surface scale on composite B at 1000 °C under humid air. (a) 5 min, (b) 11 min, (c) 20 min, (d) 39 min, (e) 60 min, (f) 72 min.

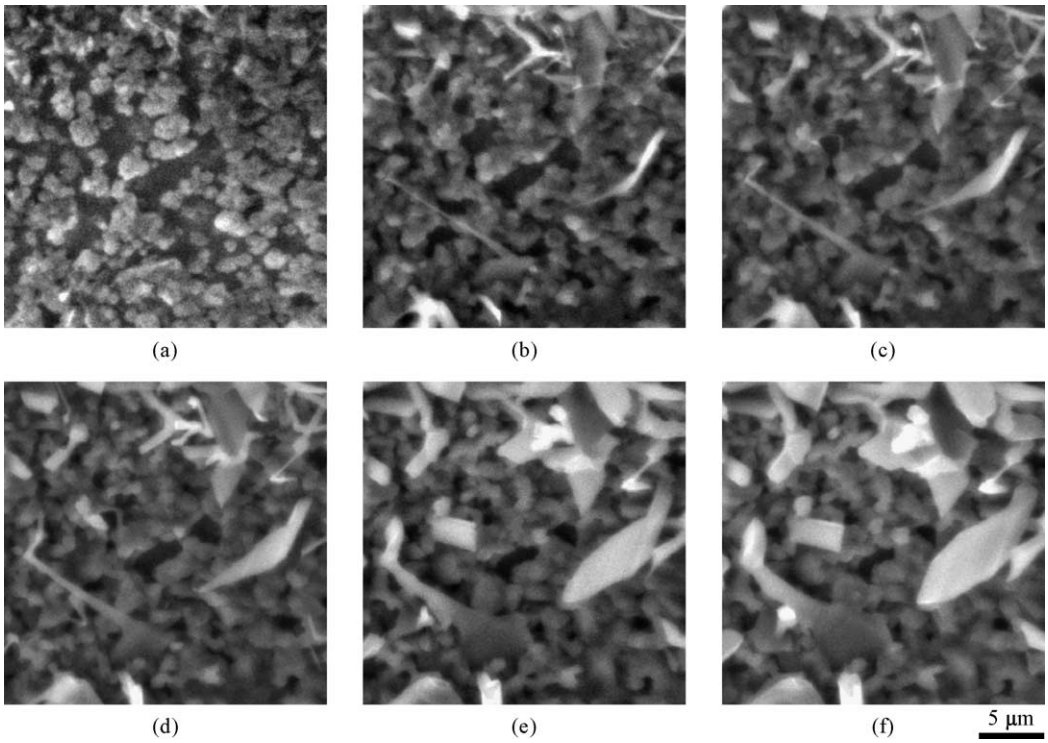

Fig. 7. Evolution of surface scale on composite B at 1100 °C under humid air. (a) 4 min, (b) 22 min, (c) 31 min, (d) 43 min, (e) 80 min, (f) 110 min.

crystals. In the course of oxidation of composite B at 1000 °C, however, the platelets did not disappear. The platelets grew to micrometer size (Fig. 6b–f) and covered the entire surface after approximately 72 min. This is a major difference compared to composite A where the platelets disappeared at 1000 °C and only equiaxial TiO_2 grains coarsened afterwards (cf. Fig. 3).

From the in situ oxidation experiments under humid air at 1100 °C (Fig. 7) it is evident that the growth of equiaxial and plate-like grains occur simultaneously in composite B. After a few minutes at 1100 °C (Fig. 7a), large areas of silicon nitride matrix (dark contrast) remained uncovered, and small TiO_2 crystals formed only on the surface of TiN particles. Even though most TiO_2 grains were equiaxial, some elongated crystals were occasionally observed (left side top and bottom). On further oxidation (less than 2 h in Fig. 7b–f), the elongated particles grew to micrometer size platelets and partially covered the underlying scale of equiaxial rutile. At the same time, lateral growth and coalescence of the equiaxial grains occurred within the underlying layer. After 110 min (Fig. 7f), some residual uncovered silicon nitride surface areas (dark contrast) were still visible. The equiaxial TiO_2 grain size reached up to 2 µm. At the same temperature in half of the time (56 min, cf. Fig. 5f), the surface of composite A had

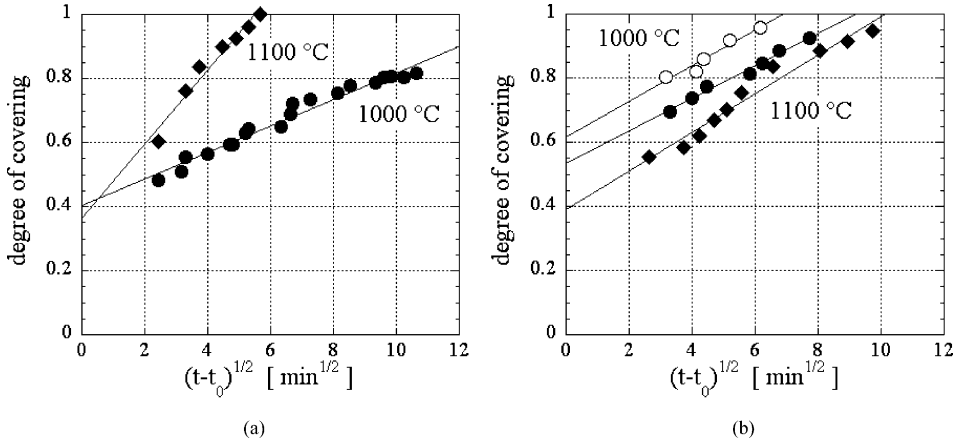

Fig. 8. Degree of covering of the surface of Si_3N_4–TiN ceramics during in situ oxidation as a function of the square root of time: (a) composite A under humid air at 1000 and 1100 °C; (b) composite B at 1000 and 1100 °C. Full markers indicate experiments under humid air; empty markers under dry air.

been completely covered, and distinctly larger TiO_2 grains had formed.

The observed coarsening, faceting and discontinuous shape changes of rutile in the surface scale are only possible by extremely rapid matter transport and can only be explained if a dissolution–precipitation process in a glass phase takes place. In this context, the term discontinuous shape change refers to the appearance and disappearance of plate-like crystals. According to our observations, initially, equiaxial grains and platelets form simultaneously. Subsequently, the scale transforms and grows to strongly faceted equiaxial particles by matter transport through the glass phase. While in composite A the high level of sinter additives provides sufficient glass phase for this process, in composite B not enough glass is present to allow fast, considerable shape changes. As a result, platelets do not transform into equiaxial grains, but instead grow to larger size in a loose superficial scale.

3.3. Kinetics of lateral scale growth

Uncovered silicon nitride surface areas can be easily distinguished from titanium nitride or titanium dioxide areas in the micrographs of the in situ oxidation experiments. A threshold on an 8-bit greyscale was used to extract the portion of uncovered silicon nitride surface area and estimate the degree of coverage (DOC) of the composite surface by TiO_2. The resulting DOC of the two composites is presented as a function of the square root of time for different in situ oxidation experiments in Fig. 8. The experimental data can be fitted into Eq. (1), which are displayed as straight lines in the figure.

$$\mathrm{DOC} = \mathrm{DOC}_0 + k\sqrt{t - t_0} \quad (1)$$

DOC_0 (DOC at $t = 0$) can be determined directly from the graphs. It is usually around 0.4, the value expected for a material with 35 vol.% TiN content. In some cases, however, an unusually high value of 0.6 was found for composite B. It should be recalled that composite B develops, under certain conditions, mainly TiO_2 platelets that hide not only the equiaxially grown TiO_2 scale, but also the silicon nitride matrix (cf. Fig. 6). Thus, the DOC curves are shifted systematically to too high values. Nevertheless, it is still possible to estimate the parabolic rate parameter k with accuracy from the slope of the curves.

Coverage of the surface by TiO_2 follows a parabolic rate law with rate constants k as obtained by the linear curve fit: composite A in humid air shows $k = 5.4 \times 10^{-3}\,\mathrm{s}^{-1/2}$ at 1000 °C and $k = 1.5 \times 10^{-2}\,\mathrm{s}^{-1/2}$ at 1100 °C. The rate constant triples from 1000 to 1100 °C. For composite B similar rate constant was found under all experimental conditions: in humid air $k = 6.5 \times 10^{-3}\,\mathrm{s}^{-1/2}$ at 1000 °C and $k = 7.8 \times 10^{-3}\,\mathrm{s}^{-1/2}$ at 1100 °C; in dry air $k = 7.2 \times 10^{-3}\,\mathrm{s}^{-1/2}$ at 1000 °C. Almost no rate increase was observed with temperature increase. The rate constants are in the same order of magnitude for all experiments. The kinetics do not depend on the applied humidity level in the atmosphere. At 1100 °C, the scale on composite A coalesces by a factor 2 faster than on composite B. It is noteworthy that scale thicknesses after the in situ oxidation, observed from cross sections,[16] were in the range of 1–2 μm in all cases.

3.4. Long-time oxidation behaviour

A general picture of the oxidation mechanism, illustrated by Fig. 9, can be drawn from the observations: At temperatures below the glass transition temperature, T_g, of the inter-

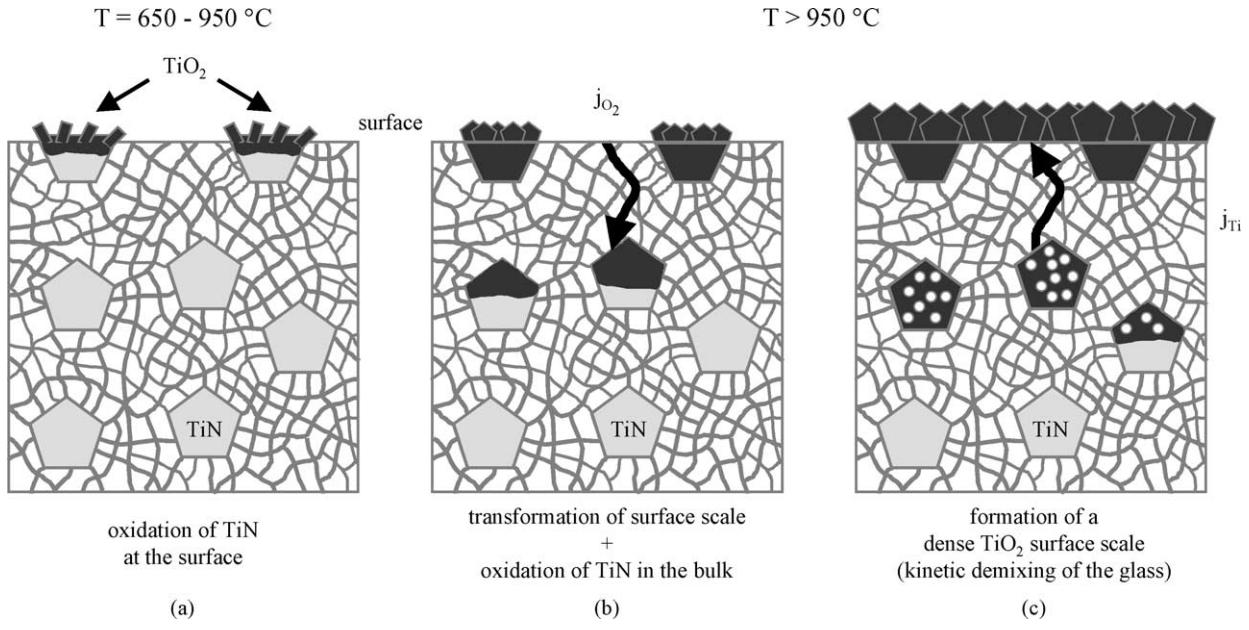

Fig. 9. Schematic view of the oxidation process mediated by the intergranular glassy film.

granular glass (approximately 950 °C), oxidation is limited to TiN grains that are exposed to the outer surface of the composite (Fig. 9a). At temperatures above the glass transition temperature, dissolution and transport processes within the intergranular glass become important and govern the oxidation process. Small titania nanocrystallites of the surface scale are dissolved in the glass and reprecipitate. As a consequence, small titania grains disappear while larger ones grow easily to their faceted low energy morphology. Through such dissolution/reprecipitation, titania platelets transform into equiaxial precipitates (Fig. 9b). Without glass, such changes in morphology are extremely difficult, because they require the formation of steps and edges and long-range matter transport, all processes that require high energies and are therefore extremely sluggish. The intergranular glass, however, is the optimum transport medium for this matter transport from one facet to the next and thus allows easy changes in morphology.

Another interesting aspect of the oxidation mechanism is that the intergranular glass is subjected during oxidation to a gradient in oxygen chemical potential μ_{O_2}. The gradient gives rise to a diffusional flux of oxygen, j_{O_2}, along the grain boundaries into the bulk of the material. Subsequently, internal titanium nitride grains are oxidized at site to titanium dioxide (Fig. 9b). Moreover, the gradient in the oxygen chemical potential acts also as a driving force for the diffusional transport of the cations (Ti, Si, Y, Al) from the bulk of the composite (low μ_{O_2}) through the glass to the surface (high μ_{O_2}).[16–18] Cations are dissolved in the inner part of the composite and diffuse to the outer surface where they are precipitated as oxides at high μ_{O_2}. The fastest diffusing species is most enriched at the surface. This phenomenon is known as kinetic demixing, the thermodynamics of which are described to some detail in a classical monograph[19] and in a recent review article.[20] In the case of Si_3N_4–TiN composites with Al_2O_3 and Y_2O_3 as sinter additives, titanium cations (network modifier in the glass) diffuse faster than silicon cations (network former in the glass), and the initially formed titanium dioxide scale grows further by titanium transport from the inner parts of the material to the outer surface. The transport process is indicated by the flux of titanium, j_{Ti}, in Fig. 9c. At higher temperatures (1400 °C), yttrium and aluminium from the sinter additives participated in the diffusion to the outer surface, enriched there, and were found together with titania in the surface scale.[17]

Several observations indicate that the intergranular phase provides an important path for titania transport. Fig. 10a shows details of the partially uncovered silicon nitride matrix surface of composite B after in situ oxidation for 75 min at 1000 °C in humid air. In the upper left corner of the image, a small TiO_2 grain is visible (bright contrast). The silicon nitride (dark contrast) is interrupted by the grain boundary phase (light grey contrast). The grain boundary lines are decorated by bright droplets of approximately 50–100 nm in size. Similar features were observed for composite A. Those droplets are exsoluted titania. Considerable quantities of titania are dissolved in the intergranular glass. Upon cooling, however, the solubility limit is exceeded and small titania precipitates are formed.

Another proof for the considerable titania transport in the glass can be seen on the sample cross sections after the oxidation. Fig. 10b presents a BSE image of a polished cross section of composite A after oxidation for 24 h at 1000 °C in humid air. Several large pores (dark contrast) can be observed at the interface between the dense surface scale of titanium dioxide (light grey in the top part of Fig. 10b) and the subscale. The subscale is composed of silicon nitride matrix (dark grey) and rounded TiO_2 particles (light grey contrast). Those TiO_2 particles occupy the place of the former TiN particles, indicating that they formed directly on site. They are surrounded by a film with dark contrast that is composed of titania-rich glass. The rounded morphology of the titania particles and the surrounding glass layer clearly indicate that titania dissolves in the glass. Since most of the rounded titania particles in the oxidation subscale are smaller in size than the original TiN particles, titania must have transported through the glass to the outer titania surface scale. It is noteworthy that the oxidation of titanium nitride to titanium dioxide is accompanied by an increase of the molar volume by a factor of 1.64 (from 11.4 cm^3/mol for TiN to 18.8 cm^3/mol for TiO_2). As the volume of a second phase particle is confined by the sur-

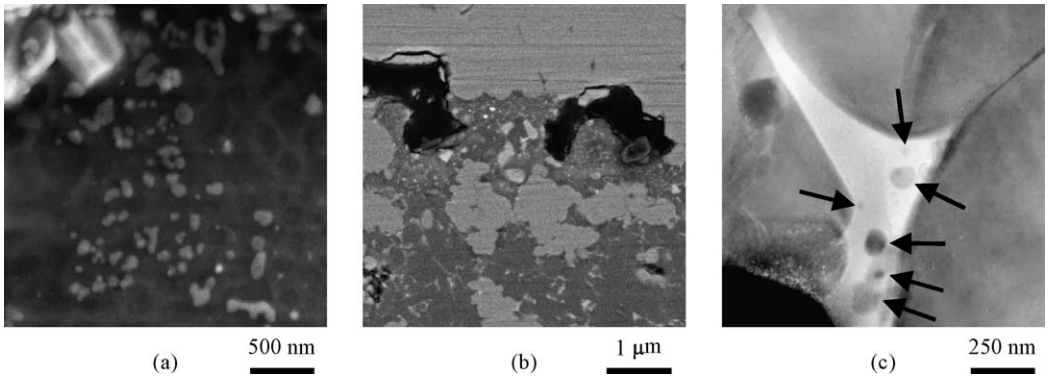

Fig. 10. (a) SE image of a detail on the surface of composite B after 75 min at 1000 °C under humid air. (b) BSE image of cross section of composite A after 24 h at 1000 °C. (c) TEM dark-field image of surface scale formed on composite A after 24 h at 1000 °C.

rounding Si_3N_4 ceramic, reaction-related stresses have to be relaxed either by viscous flow or by diffusion. Even though viscous flow may accommodate part of the volume change, the residual stresses constitute an additional driving force for the dissolution of TiO_2 into the glass and its diffusion to the outer surface. In addition, important porosity may develop in the subscale. In the scheme of Fig. 9c porosity is indicated by white circles in regions of former titanium nitride.

The TEM dark-field image in Fig. 10c shows a large quantity of intergranular glass (homogeneous bright contrast) in the interfacial area between the TiO_2 surface scale and the subscale. Several rounded rutile particles (grey contrast, marked by arrows) and small yttrium- and aluminium-containing precipitates (100 nm in size) are visible in the glass. The rounded surfaces are another evidence of the crucial role that the glass plays in the oxidation mechanism.

From the above discussion it is understandable that titania dissolution in the subscale and changes in titania precipitate morphology were mainly observed in composite A, that initially after processing contains a larger quantity of intergranular glass phase, and not in composite B. After processing, composite B showed only very thin intergranular glass films, and the global alumina/yttria-content was apparently not sufficient to form enough glass to redissolve the nanoplatelets of titanium dioxide. For the same reason the grains size of the equiaxially grown titanium dioxide particles remained much smaller in composite B.

The kinetics of scale coalescence did not differ much between the composites at 1000 °C. A similar result was found for long-time oxidation at 1000 °C.[17] At slightly higher temperature, 1100 °C, diffusion in the glass phase became more important, and composite A exhibited accelerated oxidation kinetics. In composite B with low glass phase content, no such acceleration was observed because the glass quantity was not sufficient to provide significant transport paths.

4. Conclusions

By in situ oxidation experiments in an environmental scanning electron microscope it was shown that the oxidation of Si_3N_4–TiN composites starts at around 650 °C with the formation of nanocrystalline titania particles on TiN particles that are exposed to the outer surface. Oxidation does not proceed any further as long as the temperature remains below the glass transition temperature of the intergranular glass (approximately 950 °C in the case studied with Al_2O_3–Y_2O_3 sinter additives). Above the glass transition temperature, the oxidation behaviour is governed by dissolution and diffusional transport in the intergranular glass. The glass acts as a solvent and transport medium that coalesces and coarsens the TiO_2 surface scale. Improved resistance to high-temperature oxidation is observed if the amount of intergranular glass is kept low. No dependence of the oxidation kinetics on the humidity of the atmosphere was noted. By tailoring amount and composition of the intergranular glass it should be possible to design Si_3N_4–TiN composites that withstand higher temperatures for longer time.

Acknowledgements

A part of this work was supported by the European Commission under contract number HPRN-CT-2000-00044. Composite materials were provided by Professor Martine Desmaison-Brut (University of Limoges, France) and Dr. Alida Bellosi (ISTEC-CNR, Faenza, Italy). The authors are grateful to John Hunt (Cornell Center for Materials Research, Ithaca, NY, USA) for support in ESEM-3 experiments.

References

1. Bellosi, A., Tampieri, A. and Liu, Y. Z., Oxidation behaviour of electroconductive Si_3N_4–TiN composites. *Mater. Sci. Eng. A*, 1990, **127**, 115–122.
2. Bellosi, A., Guicciardi, S. and Tampieri, A., Development and characterization of electroconductive Si_3N_4–TiN composites. *J. Eur. Ceram. Soc.*, 1992, **9**, 83–93.
3. Gogotsi, Y. G., Review—particulate silicon nitride-based composites. *J. Mater. Sci.*, 1994, **29**, 2541–2556.
4. Liu, C. C. and Huang, J. L., Microelectrode discharge machining of TiN/Si_3N_4 composites. *Br. Ceram. Trans.*, 2000, **99**, 149–152.
5. Backhaus-Ricoult, M. and Gogotsi, Y. G., Identification of oxidation mechanisms in silicon nitride ceramics by transmission electron microscopy studies of oxide scales. *J. Mater. Res.*, 1995, **10**, 2306–2321.
6. Guerin, V. and Backhaus-Ricoult, M., Comparision of the high temperature oxidation mechanisms of additive-free, MgO and MgO + Al_2O_3 containing silicon nitride ceramics. *J. Mater. Proc. Manufact. Sci.*, 1998, **7**, 23–49.
7. Backhaus-Ricoult, M., Guerin, V., Huntz, A. M. and Urbanovitch, V. S., High temperature oxidation behaviour of high-purity α-, β-, and mixed silicon nitride ceramics. *J. Am. Ceram. Soc.*, 2002, **85**, 385–392.
8. Gogotsi, Y. G. and Porz, F., The oxidation of particulate-reinforced Si_3N_4–TiN composites. *Corrosion Sci.*, 1992, **33**, 627–640.
9. Graziani, T., Baxter, D. J. and Bellosi, A., The oxidation of Si_3N_4–TiN ceramics in air-1 vol.%SO_2. *Key Eng. Mater.*, 1996, **113**, 123–134.
10. Deschaux-Beaume, F., Frety, N., Cutard, T. and Colin, C., A phenomenological model for high temperature oxidation of Si_3N_4–TiN composites. *Mater. Sci. Forum*, 2001, **372**, 403–410.
11. Deschaux-Beaume, F., Cutard, T., Frety, N. and Levaillant, Ch., Oxidation of a silicon nitride-titanium nitride composite: microstructural investigations and phenomenological modeling. *J. Am. Ceram. Soc.*, 2002, **85**, 1860–1866.
12. Klein, R., Medri, V., Desmaison-Brut, M., Bellosi, A. and Desmaison, J., Influence of additives content on the high temperature oxidation of silicon nitride based composites. *J. Eur. Ceram. Soc.*, 2003, **23**, 603–611.
13. Messier, D. R., Preparation and properties of Y-Si-Al-O-N glasses. *Int. J. High Technol. Ceram.*, 1987, **3**, 33–41.
14. Weldon, L. M., Hampshire, S. and Pomeroy, M. J., Joining of ceramics using oxide and oxynitride glasses in the Y-Sialon system. *J. Eur. Ceram. Soc.*, 1997, **17**, 1941–1947.
15. Becher, P. F., Waters, S. B., Westmoreland, C. G. and Riester, L., Compositional effects on the properties of Si-Al-RE-based oxynitride glasses (RE = La, Nd, Gd, Y, or Lu). *J. Am. Ceram. Soc.*, 2002, **85**, 897–902.

16. Feldhoff, A., Backhaus-Ricoult, M., Trichet, M. F., Mazerolles, L., Desmaison-Brut, M. and Bellosi, A., Microstructure des couches d'oxydation de composites Si_3N_4–TiN oxydés ous air sec ou humide. In *Proceedings Matériaux 2002*, October 2002, CD-ROM, ISBN 2-914279-08-6.
17. Feldhoff, A., Trichet, M. F., Mazerolles, L. and Backhaus-Ricoult, M., High-temperature oxidation of Si_3N_4–TiN composites: mechanisms and kinetics. In *Proceedings 203rd Meeting of the Electrochemical Society, PV 2003-16, High Temperature Corrosion and Materials Chemistry IV*, ed. E. Opila, P. Hou, T. Maruyama, B. Pieraggi, M. McNallan, D. Shifler and E. Wuchina. The Electrochemical Society, Pennington, NJ, 2003, pp. 377–386.
18. Feldhoff, A., Mazerolles, L., Trichet, M. F. and Backhaus-Ricoult, M., High temperature oxidation of Si_3N_4–TiN composites in dry and humid air. In *Proceedings CIMTEC 2002—10th International Ceramics Congress & 3rd Forum on New Materials, Part A*, ed. P. Vincenzini. Techna srl., Faenza, 2003, pp. 283–290.
19. Schmalzried, H., *Chemical Kinetics of Solids*. VCH Weinheim, 1995, pp. 183–207.
20. Martin, M., Materials in thermodynamic potential gradients. *J. Chem. Thermodyn.*, 2003, **35**, 1291–1308.